

What You Don't Know *Can Hurt You*: How Well do Latent Safety Filters Understand Partially Observable Safety Constraints?

Matthew Kim^{*1}, Kensuke Nakamura^{*2}, Andrea Bajcsy²

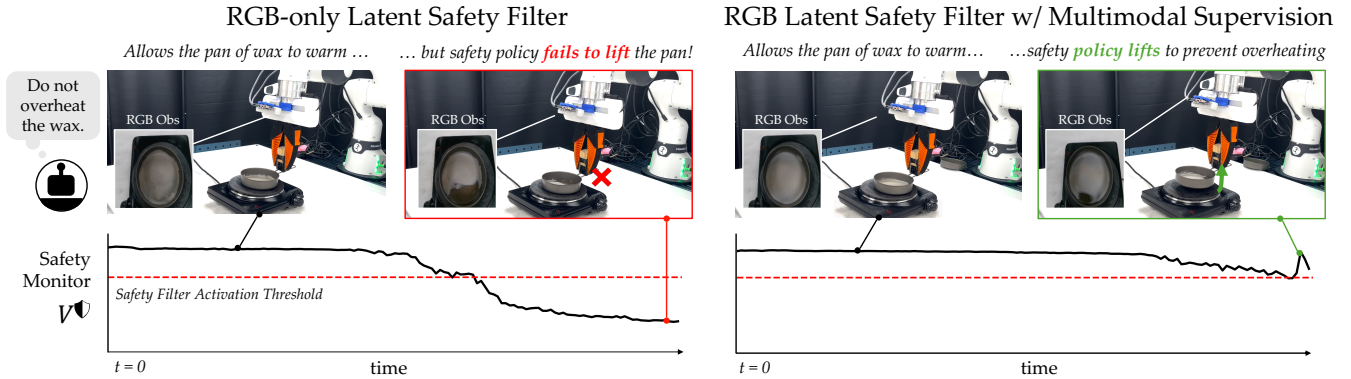


Fig. 1: We design a series of controlled experiments to test how latent safety filters behave under partially observable constraints. *Left*: We find that safety filters that rely on latent state representations trained-on and deployed-with only RGB inputs behave unreliably when they must enforce constraints, such as temperature limits, that are not easily observable. *Right*: Training with rich, safety-relevant multimodal supervision shapes the latent state representation to enable safe control (e.g., lifting the pan before overheating), even when the robot is deployed with only RGB inputs at runtime.

Abstract—Safe control techniques, such as Hamilton-Jacobi reachability, provide principled methods for synthesizing safety-preserving robot policies but typically assume hand-designed state spaces and full observability. Recent work has relaxed these assumptions via *latent-space* safe control, where state representations and dynamics are learned jointly through world models that reconstruct future high-dimensional observations (e.g., RGB images) from current observations and actions. This enables safety constraints that are difficult to specify analytically (e.g., spilling) to be framed as classification problems in latent space, allowing controllers to operate directly from raw observations. However, these methods assume that safety-critical features are observable in the learned latent state. We ask: *when are latent state spaces sufficient for safe control?* To study this, we examine temperature-based failures, comparable to overheating in cooking or manufacturing tasks, and find that RGB-only observations can produce myopic safety behaviors, e.g., avoiding *seeing failure* states rather than preventing failure itself. To predict such behaviors, we introduce a mutual information-based measure that identifies when observations fail to capture safety-relevant features. Finally, we propose a multimodal-supervised training strategy that shapes the latent state with additional sensory inputs during training, but requires no extra modalities at deployment, and validate our approach in simulation and on hardware with a Franka Research 3 manipulator preventing a pot of wax from overheating. Project Webpage: <https://cmu-intentlab.github.io/multisafe/>

I. INTRODUCTION

Safe control techniques—like Hamilton Jacobi (HJ) reachability [1], control barrier functions [2]–[4], and model

predictive shielding [5]–[7]—are principled mathematical frameworks for computing feedback policies that prevent complex dynamical systems from violating constraints. However, these methods traditionally assume perfect state observability and hand-designed state spaces, dynamics models, and safety constraints.

Recent work [8], [9] demonstrated that HJ reachability can be generalized to the *learned state spaces* and *learned dynamics models* of generative world models [10]–[12]. World models jointly learn a latent state representation, dynamics, and belief distribution over the latent state by reconstructing future high-dimensional observations from current observations and actions. This shift away from hand-crafted models has enabled safety constraints that are difficult to specify analytically (e.g., spilling) to instead be framed as classification problems in the latent space. Safety controllers can then be computed in the world model’s “imagination” to avoid these classified failure states and, at test time, operate directly on high-dimensional inputs (e.g., RGB images) via their latent encodings. We refer to this paradigm as *latent safety filters*: failure detection and corrective policies computed entirely in a learned latent space.

Despite promising early results with latent safety filters, thus far, they have operated under a key assumption: the safety-relevant features of the environment are observable from the training data used to construct the latent state and dynamics. However, this assumption does not always hold in practice. Classical control methods circumvent this by assuming *a priori* knowledge of all relevant safety-critical state variables (e.g., positions, velocities, temperatures), and account for uncertainty over this known state space via

^{*}These authors contributed equally to this work. ¹ UC San Diego. mak009@ucsd.edu. ²Carnegie Mellon University. {kensuken, abajcsy}@andrew.cmu.edu.

traditional state estimators, such as Kalman filters [13]. In contrast, the world model’s state representation is learned primarily from reconstruction and prediction objectives, with no guarantee that the safety-critical state variables are represented in the first place. Consequently, when using these world models to compute latent safety filters, it is unclear whether the latent representation is expressive enough to discriminate between safe and unsafe outcomes, potentially undermining the safety-preserving fallback policy itself.

This gap motivates our central question:

When are safety constraints observable in latent state spaces, and how do latent safety filters behave when they are not?

In this paper, we systematically investigate this question by selecting experimental settings where we can control the degree of constraint observability. Specifically, we study temperature-based safety constraints, like burning or overheating, that apply to contexts such as home robotics (e.g., cooking) or manufacturing (e.g., welding). We predict these constraints may be challenging for latent world models trained solely on RGB images, but observable for models that use multimodal RGB and infrared (IR) observations.

In simulation and hardware experiments, we discover that when safety-relevant features are unobservable, the resulting safety policies make myopic decisions: for example, policies *avoid seeing* failures rather than *avoid causing* failure. To predict when the latent-space is insufficient for observing safety constraints, we present a mutual information-based measure which is theoretically motivated and empirically shows stronger separation between sufficient and insufficient latent state spaces compared to alternative classification accuracy metrics. Finally, we show that even without any perfect state supervision, training world models with multimodal data (e.g., decoding both RGB and IR images) provides dense, informative signals that shape latent representations to remain safety-predictive at deployment, even when only one modality (e.g., RGB) is available at runtime.

Statement of Contributions. To summarize, we:

- challenge the constraint observability assumption in latent-space safe control, demonstrating that when safety features are unobservable in the latent space, the resulting latent safety filter exhibits myopic behavior,
- propose that estimating the mutual information between the observations and the safety label is predictive of this myopic behavior, moreso than other classification accuracy-based metrics,
- present a multimodal training recipe that shapes the latent representation with richer sensor modalities as supervision during world model learning, but does not require extra modalities at deployment-time,
- empirically validate our hypotheses and show our *multimodal latent safety filters* on hardware on a vision-based control task with a Franka Panda 7DoF manipulator that must prevent wax from overheating.

II. RELATED WORKS

Latent World Models. A predominant approach in world modeling is to train a state representation and dynamics model using observation-reconstruction based objectives [10]–[12]. These approaches learn to predict latent states conditioned on observations and actions such that the predicted state is sufficient for reconstructing future observations. However, it has been argued that these reconstruction-based objectives force the model to attend to irrelevant details in the observations, motivating the design of world models which operate on a more minimal representation by training with inverse dynamics learning [14], [15] or reward prediction [16]–[18]. We address a complementary question of whether the high-dimensional observations used to train the latent state are sufficient to identify safety failures, and how insufficiency in this representation can undermine the reliability of downstream latent-space safe controllers.

Multimodal Data in Robotics. Leveraging data from multiple sensor modalities has been a longstanding concept in robotics. When state variables are hand-designed by engineers (e.g., positions, velocities), a rich suite of sensor fusion techniques can efficiently fuse multimodal observations (e.g., RGB, LiDAR, radar) into a single state estimate [19]–[23]. On the other hand, robot learning methods have also trained end-to-end robot policies which take multimodal data as input (such as RGB images, tactile sensors, or audio waveforms [24]–[26]) and directly predict robot actions. However, in the context of world models, most approaches have primarily leveraged only RGB images and proprioception as input data modalities. Furthermore, unlike purely performance-based robot policies, safety filters must learn both a safety fallback policy alongside a safety monitor (taking the form of a semantically meaningful value function). In this work, we introduce a world model training recipe that shapes the latent representation using multimodal data (e.g., RGB and infrared), but enables reliable safe control at deployment time with only standard sensors (e.g., RGB cameras).

III. BACKGROUND: LATENT SAFETY FILTERS

We briefly introduce the preliminaries of latent safety filters and describe the specific models we will build upon.

World Models: Latent States & Dynamics. World models learn both a latent state representation and a corresponding dynamics model directly from high-dimensional observations and robot actions. Let $\mathcal{D} = \{(o_t, a_t, l_t)\}_{t=1}^T\}_{i=1}^N$ be the world model training dataset where $o \in \mathcal{O}$ is the robot’s observations (e.g., proprioception, RGB images) and $a \in \mathcal{A}$ are robot actions (e.g., end-effector delta actions). A latent safety constraint is learned via a classifier trained with the failure labels $l \in \{\text{safe}, \text{unsafe}\}$. Throughout this work, we build upon the Dreamer [27] world model consisting of:

$$\begin{aligned} \text{Encoder: } z &\sim \mathcal{E}(z \mid \hat{z}, o), \quad \text{Dynamics: } \hat{z}' \sim f_z(\hat{z}' \mid z, a), \\ \text{Decoder: } \hat{o} &\sim \mathcal{D}(\hat{o} \mid \hat{z}), \quad \text{Failure Classifier: } l = \ell(z). \end{aligned} \tag{1}$$

Dreamer is built on a recurrent state space model trained via two self-supervised prediction objectives: minimizing the KL divergence between the prior and posterior distribution over latent states and minimizing an observation reconstruction loss that encourages the latent space to stay informative rather than collapsing. We use an open-source PyTorch implementation of Dreamer [28] and refer the reader to [27] for details.

The safety classifier $\ell(z)$ outputs a scalar value and is trained via a hinge loss parameterized by a constant $\delta > 0$:

$$\begin{aligned} \mathcal{L}(\mu) = & \frac{1}{N_{\text{safe}}} \sum_{o^+ \in \mathcal{D}_{\text{safe}}} \text{ReLU}(\delta - \ell(\mathcal{E}(o^+))) \\ & + \frac{1}{N_{\text{fail}}} \sum_{o^- \in \mathcal{D}_{\text{fail}}} \text{ReLU}(\delta + \ell(\mathcal{E}(o^-))), \end{aligned} \quad (2)$$

where $\mathcal{D} = \mathcal{D}_{\text{safe}} \cup \mathcal{D}_{\text{fail}}$ and o^+ and o^- refer to observations assigned safe and unsafe labels, respectively. We backpropagate this loss through the entire world model which, in theory, ensures that latent representation can also identify safety constraints. This objective imbues the failure classifier with semantic meaning such that $\ell(z_t) < 0 \iff l_t = \text{unsafe}$.

Training & Deploying Latent Safety Filters. Given this world model and safety classifier, we learn a latent safety filter by solving a time-discounted latent Hamilton-Jacobi-Bellman equation [8], [9], [29]:

$$V(z) = (1 - \gamma)\ell(z) + \gamma \min\{\ell(z), \max_{a \in \mathcal{A}} \mathbb{E}_{f_z} V(f_z(z, a))\}, \quad (3)$$

which we solve using the actor-critic Deep Deterministic Policy Gradient (DDPG) algorithm [30], [31]. The fixed point of this Bellman backup yields the two quantities which make up a safety filter: a fallback policy, $\pi^\bullet : \mathcal{Z} \rightarrow \mathcal{A}$ which maximally drives the system away from violating safety constraints, and a value function $V^\bullet : \mathcal{Z} \rightarrow \mathbb{R}$ whose sign carries semantic meaning (negative values correspond to latent states that will inevitably violate safety even following the maximally safe policy π^\bullet [1], [32]). This enables safety filtering in the latent space via a least-restrictive control law:

$$a^{\text{exec}} := \mathbb{1}\{V^\bullet(z') > \epsilon\} \pi^{\text{task}} + \mathbb{1}\{V^\bullet(z') \leq \epsilon\} \pi^\bullet(z). \quad (4)$$

where $z' \sim f_z(z, \pi^{\text{task}}(z))$ for some nominal policy π^{task} . While in theory the zero-level set is sufficient for preserving safety, practitioners often use a small positive constant ϵ to account for approximation error of the value function [33].

IV. WHAT DO LATENT SAFETY CONTROLLERS DO WITHOUT CONSTRAINT OBSERVABILITY?

A central assumption of latent safe control [8], [9] is that safety-critical features are observable in the latent state; i.e., that reconstruction-based world model training will result in latent states that are predictive of safety failures. In this section, our controlled experiments in simulation and hardware reveal that violating this assumption can result in unsafe or myopic control behavior.

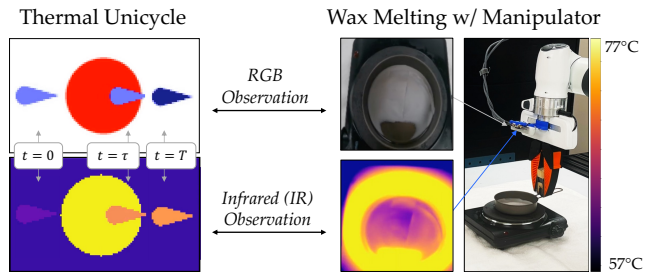


Fig. 2: **Experiment Testbeds.** In simulation (left) and hardware (right) we control data from two sensors: RGB and infrared (IR) camera. In our controlled experiments, the ground-truth safety-relevant state variable is heat, which is more observable from the IR data than the RGB.

A. Illustrative Example: Thermal Unicycle

For a low-dimensional running example, we simulate a planar vehicle which can navigate into a “hot plate” region (left, Fig. 2). The vehicle is allowed to warm up but it cannot heat up too much or it will burn.

Privileged State & Dynamics. We model the ground-truth robot system as a 4D unicycle dynamical system augmented with its temperature. The state is the ground-truth position, orientation, velocity, and heat, given by $x = [p_x, p_y, \theta, v, h]$ with dynamics

$$x_{t+1} = x_t + \Delta t[v \cos \theta_t, v \sin \theta_t, \omega, a, f_h(p_x, p_y)].$$

Here, the heat dynamics are modeled as

$$f_h(p_x, p_y) = \mathbb{I}\{(p_x^2 + p_y^2 < R^2)\} \alpha - \mathbb{I}\{(p_x^2 + p_y^2 \geq R^2)\} \beta,$$

where $\alpha = 0.03$ and $\beta = 0.06$ and the heat is bounded between $[0, 1]$. The “hot plate” is centered at the origin with radius $R = 0.5$. The robot’s velocity is bounded $v \in [0, 1]$, and it controls the turn rate and linear acceleration, $u := (\omega, a)$, which are bounded $\omega \in [-1.1, 1.1]$ radians per second and $a \in [-2, 2]$. The timestep $\Delta t = 0.05$ seconds. We label the vehicle as entering the failure set if the ground-truth heat value exceeds a threshold ($h > 0.8$).

Sensors. To study observability of the latent state, we carefully design two sets of $[128, 128]$ image observations based on a simulated RGB camera sensor and a simulated infrared (IR) sensor (Figure 2, left). For IR, the color of the vehicle is determined solely by its heat value h where higher h corresponds to a brighter color. This is designed to provide sufficient information for determining the ground-truth failure label. For RGB, the temperature changes are only visible *after* the robot exits the hot plate region, analogous to only seeing that a piece of toast has been burnt after flipping it over. Because of this model, decreasing h in future timesteps does not change the color of the robot. This second set of observations is designed to introduce correct correlations with the failure label, while simultaneously being insufficient for accurately determining the safety of the robot in isolation.

World Model & Safety Filter Training. We generate 4,000 observation-action trajectories for training the world

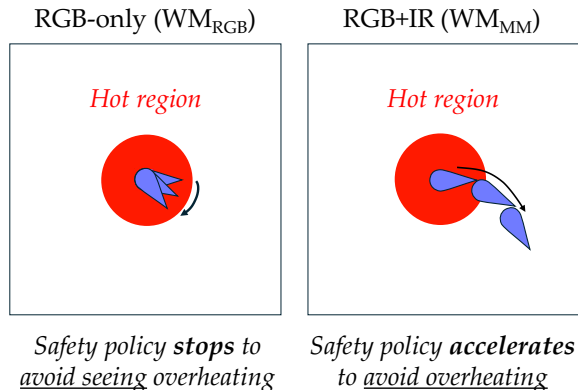


Fig. 3: **Safety Controllers without & with Observability.** In the *Thermal Unicycle* example, the robot only appears burnt in the RGB camera after it leaves the hot plate. *Left:* The safety policy is myopic when trained within a world model with an incomplete state representation: it stays in the hot region, avoiding *seeing* failure. *Right:* When the world model is trained with sufficiently rich observations (RGB + IR), the resulting safety controller makes the correct decision and accelerates out of the hot plate to prevent overheating.

model by by sampling initial states uniformly within the state bounds. At each step, control inputs are randomly drawn from their bounds. Each trajectory continues until either 1) 100 timesteps are rolled out or 2) the robot exits the valid state space. Both RGB and IR observations are recorded in every trajectory. We follow the training procedure in [8] with hinge loss parameter $\delta = 0.75$, to compute both a latent safety with an RGB-only latent safety filter, and a multimodal (RGB+IR) latent safety filter.

Results: Qualitative. Figure 3 shows the qualitative behavior of the safety filter shielding the robot when it is initialized with zero velocity inside the hot region. Since the robot begins with a cool heat state, it will take several timesteps to heat up and become burnt. The multimodal safety filter trained with IR and RGB learns to accelerate and steer out of the hot region before violating the safety constraint, due to the IR input providing strong signal of the safety-relevant heat variables. In contrast, safety violations are only observable only *after* exiting the hot region in the RGB input. Consequently, the RGB-only world model and safety classifier can only identify safety violations once the vehicle exits the hot region. This makes the resulting safe policy from optimizing (3) choose to never accelerate out of the hot region, which prevents *observing* failure in its RGB input, but fails to prevent failure itself!

B. Hardware Example: Wax Warming with a Manipulator

We also design a task in hardware where a Franka Research 3 controls a pan full of wax over a hotplate (right, Fig. 2). The safety constraint is to not overheat the wax.

Sensors, Data Collection, & Training. The manipulator has access to both a wrist-mounted FLIR Lepton infrared (IR) camera and Intel Realsense D415 RGB camera. For world model training, we collected 180 teleoperated trajectories

of a robot whose end-effector is constrained to only move along the z-axis with no rotation. The IR camera captures temperature ranges between 57 and 72°C. We automatically label failures whenever the average pixel intensity of the wax region exceeds 0.75 in the IR image corresponding to an average temperature of 77°C. This typically correlates with RGB images where part of the wax has visibly melted. Once again, we train two latent safety filters, one with RGB-only data and the other on multimodal (RGB+IR) data.

Results: Quantitative. We follow the evaluation procedure in our detailed experimental section in Sec. VI. We observe a large gap between the safety filter that has a sufficient latent representation and the one that does not. Similar to the *Thermal Unicycle* example, the multimodal safety filter in hardware consistently lifts the pan to prevent overheating, whereas the RGB-only filter fails to lift the pan 85% of the time (one such example is shown on the left of Fig. 1).

V. QUANTIFYING THE OBSERVABILITY OF SAFETY CONSTRAINTS IN THE LATENT SPACE

As shown in Sec. IV, safety fallback policies exhibit degenerate behaviors when safety-relevant features are difficult to observe in the latent state. Because the safety filter is optimized within the world model’s “imagination” (i.e., open-loop rollouts in its latent space), we aim to systematically examine the world model’s latent representation by quantifying (1) the predictive quality of its observations, (2) the ability to discriminate between safe and unsafe states from the learned latent state representation, and (3) the ability to predict future failures from the world model’s imagination.

Quantifying Observability. To estimate how observable are safety-relevant quantities from an input observation, we propose computing an estimate of the mutual information [34] between an observation X and the safety label Y . Intuitively, mutual information measures the uncertainty reduction over the random variable Y once X is observed. Formally, let X and Y as random variables drawn from a joint distribution $P(X, Y)$. Mutual information (MI) can then be defined as

$$I(Y; X) = H(Y) - H(Y | X),$$

where $H(Y)$ is the entropy and $H(Y | X)$ is the conditional entropy of the safety label Y given an observation X .

While measuring mutual information is a difficult problem in general [35], we estimate a computationally efficient Barber-Agakov lower bound [36]:

$$\begin{aligned} I(Y; X) &= H(Y) - H(Y | X) \\ &= H(Y) - H(P, Q) + D[P || Q] \\ &\geq H(Y) - H(P, Q), \end{aligned} \quad (5)$$

where $D[P || Q]$ is the Kullback-Leibler divergence and $H(P, Q)$ is the cross entropy between the true distribution $P(Y | X)$ and a variational estimate $Q(Y | X)$.

Experimental Setup. In our safety setting, it is efficient to generate empirical estimates of $H(Y)$ and $H(P, Q)$ since the safety label Y is a binary random variable. For any

Metric	Simulation			Hardware		
	RGB	IR	RGB+IR	RGB	IR	RGB+IR
$\frac{I(Y;X)}{H(Y)}$	0.182	0.909	0.903	0.221	0.801	0.853
Acc.	0.864	0.982	0.981	0.870	0.969	0.979
B. Acc.	0.738	0.966	0.976	0.626	0.983	0.988

TABLE I: **Safety-Relevant Signal in Observations.** Normalized mutual information estimates ($I(Y; X)/H(Y)$) and classification accuracies for simulated and hardware tasks.

latent world model, we freeze the pre-trained Convolutional Neural Network (CNN) encoders and train a linear probe [37] on top of these embeddings. We take separate datasets, unseen by the world models, and divide trajectories into a train/calibration/test dataset. For the *Thermal Unicycle* simulation, we are able to generate an entirely new dataset of $N = 4,000$ trajectories following the same sampling scheme used to generate the world model training dataset, and split it into 3,200/400/400 trajectories for training/calibration/evaluation. For our hardware *Wax Melting* task, we have $N = 40$ held-out trajectories, collected in the same manner as the world model training trajectories, and divide the data into 32/4/4 trajectories for training/calibration/evaluation of mutual information. The linear probe is trained to output the logits of a binary random variable via binary cross-entropy loss, and its logits are calibrated using temperature scaling [38] on the calibration data split. We estimate the cross entropy between the empirical data distribution, $\hat{P}(Y|X)$, and the predictor, $Q(Y|X)$, to obtain $H(\hat{P}, Q)$, and estimate $H(Y)$ directly from the empirical distribution of the labels, $\hat{P}(Y)$. This allows us to estimate a lower bound on how much the uncertainty over the safety label is reduced by an observation.

Q1: To what extent do different observation modalities capture safety-critical information? In simulation and hardware, we compare two world models (WMs): one trained only on RGB images (\mathbf{WM}_{RGB}) and one trained on both IR and RGB modalities (\mathbf{WM}_{MM}). Each world model encodes its observations using its respective convolutional neural networks, producing three distinct embedding vectors: e_{RGB} from the \mathbf{WM}_{RGB} and $e_{\text{RGB-MM}}$ and $e_{\text{IR-MM}}$ extracted from \mathbf{WM}_{MM} . We train four linear probes: one on top of e_{RGB} , $e_{\text{RGB-MM}}$, $e_{\text{IR-MM}}$, and $e_{\text{IR-MM}} \oplus e_{\text{RGB-MM}}$. We measure: (i) our mutual information (MI) estimate between the embedding and the safety label, normalized by $H(Y)$ to express MI as a fraction of its upper bound, (ii) standard classification accuracy of the linear probe, and (iii) balanced accuracy to account for class imbalance. Note that all metrics are bounded between 0 and 1, enabling meaningful comparisons.

Table I reports our results for $e_{\text{RGB-MM}}$, $e_{\text{IR-MM}}$, and $e_{\text{IR-MM}} \oplus e_{\text{RGB-MM}}$ (e_{RGB} omitted for space, we notice no significant deviations from $e_{\text{RGB-MM}}$). We see that our MI lower-bound metric reveals a clear gap between the informativeness of RGB-only and the IR inputs from the multimodal model.

In simulation, where RGB is designed to be insufficient for identifying safe and unsafe observations, we notice that our approximated MI lower bound is able to identify a greater separation between RGB and IR images, 0.73 nats, than

either accuracy-based metric. This trend holds on hardware, where failure labels are assigned based on IR images. This reveals that using classification accuracy can paint an incomplete picture for quantifying how much a given observation modality can detect safety-relevant quantities. On the other hand, approximated MI can clearly separate the observation modalities in both our toy *Thermal Unicycle* and hardware *Wax Melting* experiments.

Q2: To what extent does the world model’s latent state encode safety-relevant information? Reconstruction-based world models assume that observation are sufficient for useful state representations. The prior results showed that the raw observation inputs are insufficient for identifying safety constraints. However, the Dreamer world model uses a recurrent neural network backbone. This means that the latent state, z , used for policy optimization implicitly contains a history, which may be enough to accurately predict safety outcomes [39]. To test this hypothesis, we feed the world model $N = 5$ timesteps of history $(o_t, a_t)_{t=1}^N$ and report the true safe (TS), false safe (FS), false unsafe (FU), and true unsafe (TU) values alongside the cumulative F_1 score based on $\text{sign}[\ell(z_N)]$ in Table II.

Method	TS \uparrow	FS \downarrow	FU \downarrow	TU \uparrow	F_1 \uparrow
\mathbf{WM}_{RGB} (sim)	0.623	0.013	0.104	0.272	0.914
\mathbf{WM}_{MM} (sim)	0.701	0.002	0.026	0.283	0.981
\mathbf{WM}_{RGB} (HW)	0.767	0.000	0.131	0.102	0.921
\mathbf{WM}_{MM} (HW)	0.897	0.001	0.001	0.101	0.999

TABLE II: **Safety-Relevant Signal in the Latent State.** $\text{sign}[\ell(z)]$ accuracy given $N = 5$ history steps. TS = true safe, FS = false safe, FU = false unsafe, TU = true unsafe.

In simulation, \mathbf{WM}_{RGB} achieves a F_1 -score of 0.92, while \mathbf{WM}_{MM} shows adding IR increases the F_1 score to 0.98, reflecting fewer false unsafe and false safe classifications. The gap is similar in hardware, where \mathbf{WM}_{RGB} achieves an F_1 score of 0.92, while \mathbf{WM}_{MM} improves to 0.99. In short, the latent state’s ability to encode safety-relevant information mirrors the sufficiency of the observations: when the inputs fail to capture critical features, the latent representation is correspondingly degraded.

Q3: How well can world models predict safety outcomes under partial observability? Finally, even if the latent state space is sufficient for identifying the current failure label, it may lack the representational capability to *predict* future safety consequences. To study this, we compute the failure classification accuracy when rolling out the world model open-loop for 16 timesteps, after providing $N = 5$ timesteps of history from a held out evaluation set. These results have implications for safety value and policy learning from Eq. 3, since reinforcement learning takes place within the latent imagination of the world model.

We report our results in Table III. While the average classification accuracy does degrade with a less informative input modality, even \mathbf{WM}_{RGB} (HW) is able to perform relatively accurate safety classification (F_1 score of 0.90). To further

Method	TS \uparrow	FS \downarrow	FU \downarrow	TU \uparrow	F ₁ \uparrow
WM_{RGB} (sim)	0.643	0.012	0.089	0.260	0.927
WM_{MM} (sim)	0.693	0.012	0.035	0.264	0.967
WM_{RGB} (HW)	0.751	0.019	0.148	0.083	0.899
WM_{MM} (HW)	0.894	0.020	0.004	0.081	0.986

TABLE III: **Safety Outcome Prediction.** Accuracy of 16-step open-loop trajectories from $N = 5$ history steps.

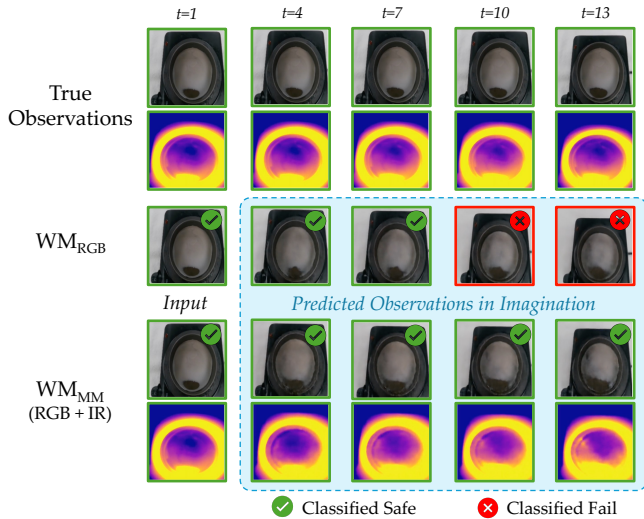


Fig. 4: **Real vs. Imagined Observations & Safety Labels.** Open-loop prediction of an evaluation subtrajectory reveals that **WM_{RGB}** incorrectly predicts the safety outcomes of actions, such as predicting that lifting the wax plate leads to failure. In contrast, observing temperature via IR images allows the **WM_{MM}** to correctly classify that this action leads to a safe outcome.

investigate the nature of any misclassifications, we visualize in Figure 4 a ground-truth observation trajectory where the robot actively lifts the wax plate. We compare the true observations to the open-loop world model’s imaginations, given the action sequence of lifting the pan, for both **WM_{RGB}** and **WM_{MM}**. We notice that while both models are able to visually predict lifting the pan, **WM_{RGB}** falsely imagines that this leads to a safety violation. In other words, the latent representation of **WM_{RGB}** has a weaker understanding how actions correlate with downstream safety outcomes.

VI. CLOSING THE OBSERVABILITY GAP WITH MULTIMODAL-SUPERVISED TRAINING

In previous sections, we showed that latent safety filters can degrade when safety-relevant features are not observable and introduced mutual information as a tool to quantify this gap. For example, while we found that RGB observations can capture visually obvious changes (such as a pan lifting), they often fail to predict necessary safety-critical state variables (like temperature). In this section, we propose a world model training strategy that leverages dense multimodal data (e.g., infrared) during offline training to shape the model’s latent state, even though only a subset of modalities (e.g., RGB) are available to the robot at deployment. We find that this offline

multimodal supervision provides a richer, more informative signal than scalar safety labels alone, producing latent states that perform more effective implicit state estimation and thus, more reliable control at deployment time.

Setup: Multimodal-Supervised World Model. We allow the Dreamer encoder to take as input only RGB images, but force the decoder to reconstruct both RGB and IR images. We denote to this as **WM_{RGB-MM}**. Note that this is different than the experiments in Sec. V where **WM_{MM}** received both RGB and IR images input into its encoder. While adding an auxiliary multimodal signal does not increase the information available at deployment, it guides the latent representation to better approximate the underlying “ground truth” state. RGB observations provide one projection of this state, but they leave many safety-relevant variables unobserved. Infrared provides a complementary projection, revealing aspects of the state that RGB alone cannot capture. By supervising the latent representation with both modalities during training, the model learns correlations between them, producing a richer latent representation that more closely approximates the true state of the system. When combined with dynamics prediction, this latent enables the inference of properties revealed by IR—even when only RGB is available at deployment—because the model has learned how these properties evolve over time. We note that this training paradigm is similar to that of Rapid Motor Adaptation [40], but with key differences: RMA requires privileged *states* as supervision for their learned *state estimator*, whereas our world model leverages privileged *observations* to learn a forward *dynamics* model of the world.

Experimental Procedure. We collect 180 trajectories of the robot interacting with the wax pan over the hotplate via teleoperation. These trajectories were of varying length and collected to contain both unsafe and safe behavior. We randomly sample 140 trajectories for training and use the remaining 40 for evaluation throughout the text. We train a Dreamer world model using an open source implementation from [28] for 10k iterations using the reconstruction and prediction objectives, then an additional 10k iterations using the failure prediction loss. We will release open source code with all hyperparameters upon acceptance. Finally, we train a latent safety filter within **WM_{RGB-MM}**.

Evaluation & Metrics. During deployment, we use a simple nominal policy, π^{task} , that grips a pan full of wax and holds it fixed over the hot plate. We deploy three latent safety filters computed in three corresponding world models: RGB-input and supervision (**WM_{RGB}**), multimodal (RGB+IR) input and supervision (**WM_{MM}**), and one with RGB inputs and multimodal supervision (**WM_{RGB-MM}**). Each filter is deployed in a least-restrictive fashion as in Sec. III with a fixed $\epsilon = 0.3$ as our threshold for all deployments. We stop each deployment trajectory after a safe lift or after the learned $\ell(z)$ falls below zero. We deploy each filter 20 times and report the safety performance in Table IV. We report the *lift rate*, which measures whether or not the fallback policy

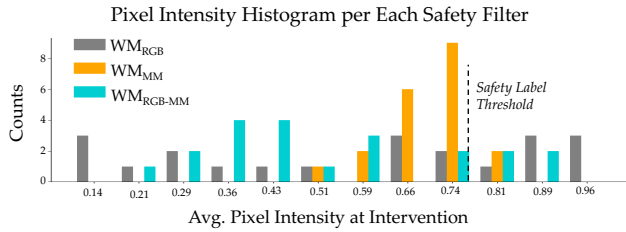


Fig. 5: Distribution of ground-truth pixel intensities when the safety filter intervenes. The \mathbf{WM}_{MM} policy that takes in IR images concentrates just prior to the safety critical threshold used for labeling, whereas \mathbf{WM}_{RGB} and $\mathbf{WM}_{\text{RGB-MM}}$ that take only RGB as input are spread more conservatively, indicating that the policy is unable to discern *when* to filter.

π^{\heartsuit} is able to learn a non-myopic recovery behavior, and the *average pixel intensity* at intervention, which measures how close to failure the system is when the filter intervenes.

Metric	World Models & Respective Safety Filters		
	\mathbf{WM}_{RGB}	\mathbf{WM}_{MM}	$\mathbf{WM}_{\text{RGB-MM}}$
Lift Rate [95% CI]	0.15 [0.04, 0.39]	1.0 [0.80, 1.0]	1.0 [0.80, 1.0]
Pixel intensity @ $V(z) = \epsilon$	0.587 ± 0.303	0.695 ± 0.073	0.522 ± 0.208

TABLE IV: **Hardware: Closed-Loop Safety Filter Performance.** We report the lift rate over 20 trials along with the 95% Wilson-CC [41] confidence interval. We find statistically significant evidence that \mathbf{WM}_{RGB} underperforms the other methods, as it is the only method unable to reliably lift the wax plate. We find that \mathbf{WM}_{MM} consistently intervenes just prior to entering the failure region (pixel intensity exceeding 0.75), whereas $\mathbf{WM}_{\text{RGB-MM}}$ is spread more widely. We hypothesize this is due to the inability to directly observe safety-relevant quantities.

Q4: How much does multimodal supervision during training shape latent state representations? We measure the normalized mutual information using the $\mathbf{WM}_{\text{RGB-MM}}$ encoder to be $\frac{I(Y;X)}{H(Y)} = 0.15$ (recall from Table D), which is aligned with the results for \mathbf{WM}_{RGB} . This is as expected, since our multimodal reconstruction objective cannot fundamentally add more information to the RGB input modality. However, when measuring how much a history-conditioned latent state can predict safety, we notice $\mathbf{WM}_{\text{RGB-MM}}$ achieves an F_1 score of 0.95 (Table V), which is comparable to 0.92 for \mathbf{WM}_{MM} . Finally, the open-loop predictions F_1 score of $\mathbf{WM}_{\text{RGB-MM}}$ in Table V once again closely matches the \mathbf{WM}_{MM} baseline at 0.94. These results suggest the latent state can be shaped for better safety prediction without added deployment inputs.

In Table IV we report the rates at which each safety filter is able to lift the pan, and the average pixel intensity of the hotplate at the timestep of safety filter intervention. Interestingly, while the masked training results in a safety filter that learns to transition the robot to a safer state by lifting the pan of wax, it is unable to discern *when* it

	TS \uparrow	FS \downarrow	FU \downarrow	TU \uparrow	$F_1 \uparrow$
Current State	0.821	0.000	0.077	0.102	0.955
OL Predictions	0.819	0.080	0.018	0.084	0.943

TABLE V: **Confusion Matrix for $\mathbf{WM}_{\text{RGB-MM}}$.** $\ell(z)$ classification metrics for $\mathbf{WM}_{\text{RGB-MM}}$, similar to Table II and III.

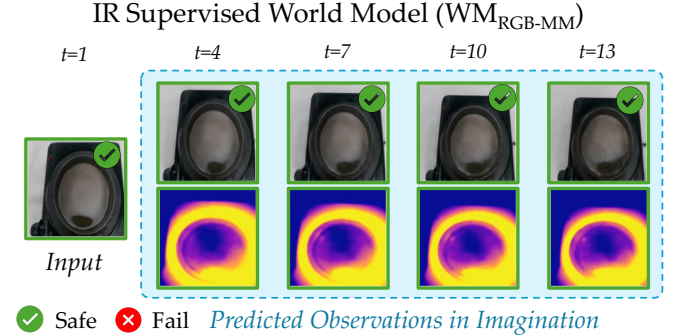


Fig. 6: **WM Supervised by Multimodal Data: Open-Loop Predictions.** Despite only taking in RGB input, multimodal training objectives enables the world model to estimate unobserved quantities (visualized via decoded IR images) and better predict safety outcomes.

should intervene due to its inability to observe the wax plate’s temperature. In practice, we find that this results in *conservative*, rather than optimistic, filtering behavior. The histogram in Fig. 5 corroborates this: the \mathbf{WM}_{MM} policy times interventions close to the safety boundary, while \mathbf{WM}_{RGB} and $\mathbf{WM}_{\text{RGB-MM}}$ trigger earlier.

However, we find that conservative value estimates do *not* always translate to a better safe policy (and a higher task success). Despite understanding that earlier intervention is better than late intervention, the \mathbf{WM}_{RGB} policy only lifts 15% of the time. This is in contrast to the $\mathbf{WM}_{\text{RGB-MM}}$ policy, which lifts 100% of the time. We attribute this gap to \mathbf{WM}_{RGB} ’s poorer understanding of how robot actions affect the underlying state quantities that determine safety. As shown in Figure 4, when the robot imagines the consequences of lifting its end-effector, \mathbf{WM}_{RGB} incorrectly imagines entering failure states (i.e., $l(z) < 0$). Thus, the resulting value function learns to penalize this latent state trajectory and fails to learn the safe recovery behavior. By simply shaping the latent representation with multimodal supervision, the $\mathbf{WM}_{\text{RGB-MM}}$ world model learns latent features that capture relative cues about safe actions as visualized in Figure 6. This allows it to choose safe actions even if it is unable to make absolute judgments about the exact moment to intervene.

VII. CONCLUSION & LIMITATIONS

In this paper, we investigate how latent safety filters can degrade when trained-on and deployed-with observations that do not directly observe safety-critical features. We find that mutual information is a useful metric for identifying observations that are predictive of safety, and that including this information to shape the latent representation of a world

model can improve downstream safety filtering behavior. Our results show that while shaping the latent representation with multimodal reconstruction objectives leads to stronger representations from which models can make relative judgments on safety, fundamental limitations on observability may still result in overly conservative safety interventions. This work is a first step toward understanding what matters for shaping latent representation for safe control and opens exciting avenues for blending representation learning and uncertainty quantification/state estimation for latent space control.

Limitations. While we propose mutual information as a metric to quantify when safety is not well captured in the latent state, an open question is how to inject the missing safety information. Our experiments are also restricted to controlled domains where the degree of observability can be precisely manipulated; in more complex environments, it is harder to characterize when latent spaces fail to encode safety. Both of these limitations are promising directions for future work. Finally, although our method is grounded in rigorous theory, future work should provide formal assurances on the composition of all the learned components.

REFERENCES

- [1] S. Bansal, M. Chen, S. Herbert, and C. J. Tomlin, "Hamilton-jacobi reachability: A brief overview and recent advances," in *2017 IEEE 56th Annual Conference on Decision and Control (CDC)*. IEEE, 2017.
- [2] A. D. Ames, S. Coogan, M. Egerstedt, G. Notomista, K. Sreenath, and P. Tabuada, "Control barrier functions: Theory and applications," in *2019 18th European control conference (ECC)*, 2019.
- [3] O. So, Z. Serlin, M. Mann, J. Gonzales, K. Rutledge, N. Roy, and C. Fan, "How to train your neural control barrier function: Learning safety filters for complex input-constrained systems," in *2024 IEEE International Conference on Robotics and Automation (ICRA)*. IEEE, 2024, pp. 11 532–11 539.
- [4] M. Kim, W. Sharpless, H. J. Jeong, S. Tonkens, S. Bansal, and S. Herbert, "Reachability barrier networks: Learning hamilton-jacobi solutions for smooth and flexible control barrier functions," *arXiv preprint arXiv:2505.11755*, 2025.
- [5] O. Bastani, "Safe reinforcement learning with nonlinear dynamics via model predictive shielding," in *2021 American control conference*. IEEE, 2021.
- [6] S. Li and O. Bastani, "Robust model predictive shielding for safe reinforcement learning with stochastic dynamics," in *2020 IEEE International Conference on Robotics and Automation*. IEEE, 2020.
- [7] H. Hu, K. Nakamura, and J. F. Fisac, "Sharp: Shielding-aware robust planning for safe and efficient human-robot interaction," *IEEE Robotics and Automation Letters*, vol. 7, no. 2, pp. 5591–5598, 2022.
- [8] K. Nakamura, L. Peters, and A. Bajcsy, "Generalizing safety beyond collision-avoidance via latent-space reachability analysis," *Robotics: Science and Systems (RSS)*, 2025.
- [9] J. Seo, K. Nakamura, and A. Bajcsy, "Uncertainty-aware latent safety filters for avoiding out-of-distribution failures," *Conference on Robot Learning (CoRL)*, 2025.
- [10] D. Ha and J. Schmidhuber, "World models," *arXiv preprint arXiv:1803.10122*, vol. 2, no. 3, 2018.
- [11] D. Hafner, T. Lillicrap, I. Fischer, R. Villegas, D. Ha, H. Lee, and J. Davidson, "Learning latent dynamics for planning from pixels," in *International Conference on machine learning (ICML)*, 2019.
- [12] G. Zhou, H. Pan, Y. LeCun, and L. Pinto, "Dino-wm: World models on pre-trained visual features enable zero-shot planning," *International Conference on machine learning (ICML)*, 2025.
- [13] R. E. Kalman, "A new approach to linear filtering and prediction problems," *Journal of Basic Engineering*, vol. 82, no. 1, 1960.
- [14] Y. Efroni, D. Misra, A. Krishnamurthy, A. Agarwal, and J. Langford, "Provably filtering exogenous distractors using multistep inverse dynamics," in *International Conference on Learning Representations*, 2022. [Online]. Available: <https://openreview.net/forum?id=RQLLzMCefQu>
- [15] A. Lamb, R. Islam, Y. Efroni, A. Didolkar, D. Misra, D. Foster, L. Molu, R. Chari, A. Krishnamurthy, and J. Langford, "Guaranteed discovery of control-endogenous latent states with multi-step inverse models," *arXiv preprint arXiv:2207.08229*, 2022.
- [16] Y. Tian, K. Zhang, R. Tedrake, and S. Sra, "Toward understanding state representation learning in muzero: A case study in linear quadratic gaussian control," in *2023 62nd IEEE Conference on Decision and Control (CDC)*. IEEE, 2023, pp. 6166–6171.
- [17] N. Hansen, H. Su, and X. Wang, "Td-mpc2: Scalable, robust world models for continuous control," in *International Conference on Learning Representations (ICLR)*, 2024.
- [18] B. Huang, C. Lu, L. Leqi, J. M. Hernández-Lobato, C. Glymour, B. Schölkopf, and K. Zhang, "Action-sufficient state representation learning for control with structural constraints," in *International Conference on Machine Learning*. PMLR, 2022, pp. 9260–9279.
- [19] S. Duan, Q. Shi, and J. Wu, "Multimodal sensors and ml-based data fusion for advanced robots," *Advanced Intelligent Systems*, vol. 4, no. 12, p. 2200213, 2022.
- [20] M. A. Lee, B. Yi, R. Martín-Martín, S. Savarese, and J. Bohg, "Multimodal sensor fusion with differentiable filters," in *2020 IEEE/RSJ International Conference on Intelligent Robots and Systems (IROS)*. IEEE, 2020, pp. 10 444–10 451.
- [21] X. Xu, L. Zhang, J. Yang, C. Cao, W. Wang, Y. Ran, Z. Tan, and M. Luo, "A review of multi-sensor fusion slam systems based on 3d lidar," *Remote Sensing*, vol. 14, no. 12, p. 2835, 2022.
- [22] R. C. Luo, C.-C. Yih, and K. L. Su, "Multisensor fusion and integration: approaches, applications, and future research directions," *IEEE Sensors journal*, vol. 2, no. 2, pp. 107–119, 2002.
- [23] S. Speth, A. Gonçalves, B. Rigault, S. Suzuki, M. Bouazizi, Y. Matsuo, and H. Prendinger, "Deep learning with rgb and thermal images onboard a drone for monitoring operations," *J. Field Robotics*, vol. 39, no. 6, pp. 840–868, 2022. [Online]. Available: <https://doi.org/10.1002/rob.22082>
- [24] L. Heng, H. Geng, K. Zhang, P. Abbeel, and J. Malik, "Vitaformer: Learning cross-modal representation for visuo-tactile dexterous manipulation," 2025. [Online]. Available: <https://arxiv.org/abs/2506.15953>
- [25] A. Thankaraj and L. Pinto, "That sounds right: Auditory self-supervision for dynamic robot manipulation," in *7th Annual Conference on Robot Learning*, 2023. [Online]. Available: <https://openreview.net/forum?id=sLhk0keiseH>
- [26] J. Mejia, V. Dean, T. Hellebrekers, and A. Gupta, "Hearing touch: Audio-visual pretraining for contact-rich manipulation," in *2024 IEEE International Conference on Robotics and Automation (ICRA)*. IEEE, 2024, pp. 6912–6919.
- [27] D. Hafner, J. Pasukonis, J. Ba, and T. Lillicrap, "Mastering diverse control tasks through world models," *Nature*, vol. 640, no. 8059, 2025.
- [28] N. Morihira, "dreamerv3-torch: Implementation of dreamer v3 in pytorch," <https://github.com/NM512/dreamerv3-torch>, 2025, accessed: 2025-01-25.
- [29] J. F. Fisac, N. F. Lugovoy, V. Rubies-Royo, S. Ghosh, and C. J. Tomlin, "Bridging hamilton-jacobi safety analysis and reinforcement learning," in *2019 International Conference on Robotics and Automation (ICRA)*, 2019, pp. 8550–8556.
- [30] T. P. Lillicrap, J. J. Hunt, A. Pritzel, N. Heess, T. Erez, Y. Tassa, D. Silver, and D. Wierstra, "Continuous control with deep reinforcement learning," 2019. [Online]. Available: <https://arxiv.org/abs/1509.02971>
- [31] J. Li, D. Lee, J. Lee, K. S. Dong, S. Sojoudi, and C. Tomlin, "Certifiable reachability learning using a new lipschitz continuous value function," *IEEE Robotics and Automation Letters*, vol. 10, no. 4, pp. 3582–3589, 2025.
- [32] K.-C. Hsu, H. Hu, and J. F. Fisac, "The safety filter: A unified view of safety-critical control in autonomous systems," *Annual Review of Control, Robotics, and Autonomous Systems*, vol. 7, 2023.
- [33] K. Leung, E. Schmerling, M. Zhang, M. Chen, J. Talbot, J. C. Gerdes, and M. Pavone, "On infusing reachability-based safety assurance within planning frameworks for human-robot vehicle interactions," *The International Journal of Robotics Research*, vol. 39, no. 10-11, pp. 1326–1345, 2020.

- [34] C. E. Shannon, "A mathematical theory of communication," *The Bell System Technical Journal*, vol. 27, pp. 379–423, 1948. [Online]. Available: <http://plan9.bell-labs.com/cm/ms/what/shannonday/shannon1948.pdf>
- [35] A. Kraskov, H. Stögbauer, and P. Grassberger, "Estimating mutual information," *Phys. Rev. E*, vol. 69, p. 066138, Jun 2004. [Online]. Available: <https://link.aps.org/doi/10.1103/PhysRevE.69.066138>
- [36] D. Barber and F. Agakov, "The im algorithm: a variational approach to information maximization," in *Proceedings of the 17th International Conference on Neural Information Processing Systems*, ser. NIPS'03. Cambridge, MA, USA: MIT Press, 2003, p. 201–208.
- [37] G. Alain and Y. Bengio, "Understanding intermediate layers using linear classifier probes," *International Conference on Learning Representations*, 2017.
- [38] C. Guo, G. Pleiss, Y. Sun, and K. Q. Weinberger, "On calibration of modern neural networks," in *Proceedings of the 34th International Conference on Machine Learning - Volume 70*, ser. ICML'17. JMLR.org, 2017, p. 1321–1330.
- [39] V. Mnih, K. Kavukcuoglu, D. Silver, A. A. Rusu, J. Veness, M. G. Bellemare, A. Graves, M. Riedmiller, A. K. Fiedjeland, G. Ostrovski, S. Petersen, C. Beattie, A. Sadik, I. Antonoglou, H. King, D. Kumaran, D. Wierstra, S. Legg, and D. Hassabis, "Human-level control through deep reinforcement learning," *Nature*, vol. 518, no. 7540, pp. 529–533, Feb. 2015. [Online]. Available: <http://dx.doi.org/10.1038/nature14236>
- [40] A. Kumar, Z. Fu, D. Pathak, and J. Malik, "Rma: Rapid motor adaptation for legged robots," 2021. [Online]. Available: <https://arxiv.org/abs/2107.04034>
- [41] R. G. Newcombe, "Two-sided confidence intervals for the single proportion: comparison of seven methods," *Statistics in Medicine*, vol. 17, no. 8, pp. 857–872, 1998.

VIII. APPENDIX

A. Hyperparameters

For all experiments, we use an open-source implementation of the Dreamerv3 Recurrent State Space Model (RSSM) [28]. Hyperparameters for the Thermal Unicycle are included in Table VI and hardware experiments in Table VII

HYPERPARAMETER	VALUE
RGB IMAGE DIMENSION	[128, 128, 3]
IR IMAGE DIMENSION	[128, 128, 1]
ACTION DIMENSION	1
STOCHASTIC LATENT	Gaussian
LATENT DIM (DETERMINISTIC)	512
LATENT DIM (STOCHASTIC)	32
ACTIVATION FUNCTION	SiLU
ENCODER CNN DEPTH	32
ENCODER MLP LAYERS	5
FAILURE PROJECTOR LAYERS	2
BATCH SIZE	16
BATCH LENGTH	64
OPTIMIZER	Adam
LEARNING RATE	1e-4
ITERATIONS	15000

TABLE VI: Sim RSSM Hyperparameters

On Hardware, we limit the action-space of the robot to z-axis translation only. However, we recording 7-dimensional actions corresponding to delta translation (3dof) / axis angle rotations (3dof), and a binary gripper action (1dof). We rescale by the max/min of the dataset so both the world model and HJ value function take actions scaled between $[-1, 1]$ for each action dimension. Data is collected at 15Hz

and downsampled to 3Hz due to the slow dynamics of wax melting.

HYPERPARAMETER	VALUE
RGB IMAGE DIMENSION	[224, 224, 3]
IR IMAGE DIMENSION	[224, 224, 1]
ACTION DIMENSION	7
STOCHASTIC LATENT	Gaussian
LATENT DIM (DETERMINISTIC)	512
LATENT DIM (STOCHASTIC)	32
ACTIVATION FUNCTION	SiLU
ENCODER CNN DEPTH	32
ENCODER MLP LAYERS	5
BATCH SIZE	16
BATCH LENGTH	64
OPTIMIZER	Adam
LEARNING RATE	1e-4
$\ell(z)$ LEARNING RATE	5e-4
ITERATIONS	20000

TABLE VII: Hardware RSSM Hyperparameters

Safety Filter Synthesis. All safety filters are obtained by approximately solving for the fixed point of a latent Hamilton Jacobi Bellman equation via off policy DDPG algorithm [30]. We parameterize the state-action value function and co-optimized safety fallback policies as an MLP which are trained via rollouts in the latent space of our world model. Unlike when using traditional simulators for RL, we 'reset' the environment by sampling random $N = 5$ length trajectory segments from our offline dataset to initialize the latent state before rolling out open-loop imagination rollouts for a maximum of 16 timesteps. This reset procedure and short-horizon rollout is to prevent excessive instability in the world model imagination. We follow [8] and take $\tanh(\lambda \ell(z))$ with $\lambda = 0.1$ as our margin function for reachability learning to smooth out the loss landscape.

We list the hyperparameters for the DDPG HJ Value function learning in Table VIII. We train each policy for 600k iterations and save checkpoints every 40k. All reported results are from the best performing checkpoint for each model (not necessarily the final checkpoint, due to minor instabilities of the RL training procedure).

HYPERPARAMETER	VALUE
ACTOR ARCHITECTURE	[512, 512, 512]
CRITIC ARCHITECTURE	[512, 512, 512]
NORMALIZATION	LayerNorm
ACTIVATION	ReLU
DISCOUNT FACTOR γ	0.9999
LEARNING RATE (CRITIC)	1e-3
LEARNING RATE (ACTOR)	1e-4
OPTIMIZER	AdamW
NUMBER OF ITERATIONS	600000
REPLAY BUFFER SIZE	40000
BATCH SIZE	512
MAX IMAGINATION STEPS	16

TABLE VIII: DDPG hyperparameters.